http://dx.doi.org/10.21577/0103-5053.20190073

J. Braz. Chem. Soc., Vol. 30, No. 8, 1707-1716, 2019
Printed in Brazil - ©2019 Sociedade Brasileira de Química

Article

The Influence of Different Ammonium Cations on the Optical Properties of Tetrakis Gd^{III} and Eu^{III} Complexes

Renata D. Adati, *[a,b] *Jorge H. S. K. Monteiro,*[a] *Lucas P. Cardoso,*[b] *Daniel H. de Oliveira,*[b] *Miguel Jafelicci Jr.*[a] *and Marian R. Davolos**[a]

[a]*Laboratório de Materiais Luminescentes, Departamento de Química Geral e Inorgânica, Instituto de Química, Universidade Estadual Paulista (Unesp), 14800-060 Araraquara-SP, Brazil*

[b]*Departamento de Química e Biologia, Universidade Tecnológica Federal do Paraná (UTFPR), 81280-340 Curitiba-PR, Brazil*

A series of tetrakis-β-diketonate $Q^+[Ln(\beta\text{-dik})_4]^-$, where Ln = Gd^{III} or Eu^{III}, Q = ammonium cations and β-dik = tta (2-thenoyltrifluoracetone) or bmdm (1-(4-*tert*-butylphenyl)-3-(4-methoxyphenyl)-1,3-propanedione) have been synthesized and characterized. The environment surrounding the Eu^{III} ion depends on the lateral groups of the ligand and on the alkyl chains of the counter ion Q. The shortest lifetime (τ) = 0.29 ms, and lowest quantum efficiencies (η) = 24%, were obtained for $(N(C_{12}H_{25})_2(CH_3)_2)^+[Eu(bmdm)_4]^-$, while $(N(C_4H_9)_4)^+[Eu(bmdm)_4]^-$ has the longest τ = 1.04 ms and η = 90%. The Judd-Ofelt intensity parameters (Ω_2 and Ω_4) strongly changes for tta series pointing to stronger ion-dipole interactions between the $-CF_3$ group with the ammonium cations. The agreement between the experimental results of photoluminescence and theoretical data suggests that the geometries optimized by the Sparkle model are correct. These results point to potential candidates for building up Langmuir-Blodgett (LB) luminescent films, since it is possible to maximize the intermolecular interactions and the photoluminescent properties of tetrakis Ln^{III} complexes.

Keywords: tetrakis-β-diketonate, ammonium cations, photoluminescent properties, semi-empirical methods, europium

Introduction

The characteristic emission lifetimes in the range μs-ms and the narrow emission bands of the Ln^{III} compounds are very attractive for applications such as displays, sensors and photoluminescent labels in biological systems.[1-5] Due to the Laporte forbidden 4f-4f transitions, the absorption of energy occurs through a sensitizer (usually an organic ligand), also called antenna, and then transferred to the Ln^{III} that emits in a characteristic wavelength.[6] Modifications in the ligand structure affect not only the energy transfer ligand → Ln^{III} efficiency, but also sensing of oxygenated and biological species, solubility and thin films stability, for example.[7-12] β-Diketonate (β-dik) ligands have been used as ligands for Ln^{III} sensitization due to the simple synthesis and high emission intensity of the Ln^{III} complexes and formation of stable tris ($[Ln(\beta\text{-dik})_3(H_2O)_2]$) or tetrakis ($[Ln(\beta\text{-dik})_4]^-$) complexes. In the case of the tetrakis $[Ln(\beta\text{-dik})_4]^-$ complexes the negative electric charge is balanced by an alkali metal ion[13,14] or an organic cation.[15,16]

The main interest in Ln^{III}-β-diketonate complexes lies in their photoluminescent properties. From the absorption or luminescence spectra, Judd-Ofelt (JO) theory has the ability to predict the oscillator strengths, estimates of quantum efficiencies and excited state radiative lifetimes in terms of intensity parameters Ω_t (t = 2, 4, 6).[17-19] Typically, the Ω_2 parameter is associated with short-range coordination effects. The higher polarization and asymmetry of the Ln^{III}-β-diketones, the larger Ω_2 value is expected. Nevertheless, the other two parameters $\Omega_{4,6}$ depend on long-range effects. JO theory has become crucial to evaluating the performance of the luminescent materials in terms of symmetry around Eu^{III} ion.[19-21]

Tris- and tetrakis-β-diketonate Ln^{III} complexes have been widely used as the emitting layer in organic light-emitting diodes (OLEDs) due to the high intensity and monochromatic emission.[22] The last one is known to be promising, due to their higher thermal and chemical

*e-mail: renataadati@utfpr.edu.br; davolos@iq.unesp.br

stabilities, luminescence lifetimes, the cross-section of photon absorption and charge carrier trapping and luminescence quantum yields than the widely studied tris-complexes. Biju *et al*.[23] reported that β-diketonate ligands containing hole-transporting carbazole group and π-spacer extended the excitation window of the Eu^{III}-complex. The improved carrier transport properties and electron injection into the emitting layer resulted in emission from a host free device, also the presence of carbazol-9-yl-biphenyl group in the ligand reduced the turn-on voltage and improved device efficiency significantly. Martins *et al*.[24] observed a lowering in the voltage operation, compared to other devices, using Eu-tetrakis β-diketonate dimeric complexes as the active layer in a solution-processed OLED.

Besides the potential of the Ln^{III} luminescent complexes to be used as emissive layer, transferring the compound into a solid substrate is the biggest challenge. The most used technique is the high vacuum-based evaporation technique that has drawbacks such as the long time to deposit the layers, energetically inefficient and sometimes decomposition of the Ln^{III} complex.[22,25,26] In this sense, the Langmuir-Blodgett (LB) technique offers some advantages such as the possibility for obtaining ultrathin films with layered structures and thickness controlled at the molecular level.[27-30] This technique consists of spreading a single layer of molecules on a liquid surface, typically water (denoted Langmuir monolayer), and then transferring onto a solid support to form a thin film in a vertical position. Repetition of the process, by successive immersion-emersion of the substrate into the subphase, yields multi-layered structures, building up a Langmuir-Blodgett film.[31,32]

The use of the LB technique has proven to be an excellent alternative to the evaporation methods in the preparation of ultrathin films for display and optical applications.[33,34] Using this technique, well-ordered layers in OLEDs can be obtained with improved performance,[35] longer lifetimes of the device and reduced thickness.[33] Pavier *et al*.[36] described that electroluminescent devices can be made using 15 LB monolayers of Nd^{III} or Dy^{III} complexes. Generation of the Eu^{III} complex *in situ* is also possible by using aqueous $EuCl_3$ solution as subphase and dispersing a biphenylpyrazine derivative ligand with short alkyl chain.[37] The Langmuir film of the Eu^{III} complex generated was transferred (40 layers) to a substrate and was used as emissive layer in an organic double heterostructure device. The emission spectra obtained using electro or photoluminescence are in good agreement, which demonstrated that the bimolecular layer acts as molecular-size emissive layer.[37]

The use of the LB technique has shown that control over the packing density of molecules is associated with intermolecular forces (ion-ion, ion-dipole or dipole-dipole interactions). Yan and co-workers[18] reported that long chain ligands (phthalate monoester) are suitable antennas for Tb^{III} and Dy^{III} and also improved the formation of LB films.[18] We reported that stable Langmuir monolayers and LB films could be obtained using the amphiphilic Eu^{III} complex $(N(C_{12}H_{25})_2(CH_3)_2)^+[Eu(tta)_4]^-$. The stable Langmuir monolayers formed by this complex at the air/water interface indicated that the packing of the complex is dominated by the chemical interactions between cation $(N(C_{12}H_{25})_2(CH_3)_2)^+$) and anion ($[Eu(tta)_4]^-$) that was confirmed using semi-empirical methods.[38] This simple strategy to use organic cations, such as long alkyl chain ammonium or *N*-alkylpyridinium cations, can make possible the formation of LB films of virtually any compound by adequate selection of cation and anion to maximize the intermolecular interactions.[38-41]

Therefore, the study of the counterion-tetrakis Ln^{III} complexes interaction can contribute to the development of new efficient Ln^{III} luminescent complexes that can form stable LB films and be applied as emissive layers in displays. In this context, we report the synthesis, characterization and influence of the counterion in the photoluminescent properties of tetrakis Eu^{III} or Gd^{III} complexes with the general formula $Q^+[Ln(\beta\text{-dik})_4]^-$ (β-dik = 2-thenoyltrifluoracetone (tta) or 1-(4-*tert*-butylphenyl)-3-(4-methoxyphenyl)propane-1,3-dione (bmdm)) neutralized by different ammonium cations Q (tetraethylammonium, tetrabutylammonium, and didodecyldimethylammonium) containing short, intermediate or long alkyl chain.

Experimental

All commercially obtained reagents were of analytical grade and were used as received, $EuCl_3$ and $GdCl_3$ were obtained by dissolving the respective oxide in concentrated hydrochloric acid.[42] Unless otherwise indicated, all data were collected at a constant temperature of 25 ± 1 °C. The chemical stoichiometries of the complexes were suggested by carbon, hydrogen and nitrogen elemental analysis (PerkinElmer 2400) and Ln^{III} titration using a standard 0.01 mol L^{-1} ethylenediaminetetraacetic acid (EDTA) solution. The thermogravimetric analysis (TA instruments SDT 2960) were carried out using a synthetic air flow (100 mL min^{-1}) under a heating rate of 10 °C min^{-1}. Fourier transform infrared spectroscopy (FTIR PerkinElmer 2000) data were obtained in transmission mode using KBr pellets.

Synthesis of $Q^+[Ln(\beta\text{-dik})_4]^-$

4.2 mmol β-dik (β-dik = tta or bmdm), 1.2 mmol ammonium salt, Q = $(N(C_2H_5)_4)^+$, $(N(C_4H_9)_4)^+$ or

$(N(C_{12}H_{25})_2(CH_3)_2)^+$ were dissolved in ethanol until complete solubilization. 1.0 mmol $LnCl_3 \bullet 6H_2O$ (Ln = Eu^{III} or Gd^{III}) was slowly added to previous solution and the pH was adjusted to ca. 5 by adding 4.2 mL NaOH solution (0.1 mol L^{-1}) in a one-to-one molar ratio. The system was kept under stirring and heating for ca. 3 h at 50 °C until the complete precipitation of the $Q^+[Ln(\beta\text{-dik})_4]^-$ complexes. The solid was filtered out, washed with ethanol and dried in a vacuum oven at room temperature.[42] The compounds were characterized by elemental analysis (Table 1).

Photophysical characterization

The photoluminescence data were obtained in a Fluorolog-3 spectrofluorometer (Horiba FL3-222), with double-gratings (1200 gr mm^{-1}, 330 nm blazed) in the excitation monochromator and double-gratings (1200 gr mm^{-1}, 500 nm blazed) in the emission monochromator. An ozone-free xenon lamp of 450 W was used as a radiation source. The excitation spectra were obtained between 200-600 nm monitoring the $^5D_0 \rightarrow {}^7F_2$ transition at ca. 298 K. All the excitation spectra were corrected in real time according to the lamp intensity and the optical system of the excitation monochromator using a silicon diode as a reference detector. The emission spectra were carried out between 400-750 nm at ca. 77 K using the front face mode at 22.5°. All emission spectra were corrected according to the optical system of the emission monochromator and the photomultiplier response (Hamamatsu R928P). The time-resolved phosphorescence emission spectra of the analogous Gd^{III} complexes were obtained at ca. 77 K using a phosphorimeter system (Jobin Yvon, FL-1040 model) with delay of time long enough to get only the emission from triplet level of the ligands. The energy values of the ligand triplet level were obtained fitting a tangent to the highest energy edge of the emission spectra. The emission decay curves were obtained with a pulsed 150 W xenon lamp using a phosphorimeter system (Jobin Yvon, FL-1040 model) at ca. 298 K. The Judd-Ofelt (JO) intensity parameters (Ω_2 and Ω_4) and the efficiency parameters (A_{rad} ($^5D_0$ radiative decay rates), A_{tot} (total emission rate) and η (quantum efficiency)) were calculated using the equations 1, 2 and 3, respectively, and widely described in the literature.[43]

$$\Omega_\lambda = \frac{3\hbar c^3 A_{0\lambda}}{4e^2\omega^3\chi\left\langle {}^7F_J \left\| U^{(\lambda)} \right\| {}^5D_0 \right\rangle^2} \quad (1)$$

where: $\hbar$ is the Planck's constant over 2π; c is the speed of light; $A_{0\lambda}$ is the radiative rate, given by the equation 2, e is the electronic charge; ω is the angular frequency of the transition; χ is the Lorentz local field correction; $\left\langle {}^7F_J \left\| U^{(\lambda)} \right\| {}^5D_0 \right\rangle^2$ is the squared diagonalized matrix values.

$$A_{0\lambda} = A_{01}\left(\frac{I_{0\lambda}}{I_{01}}\right)\left(\frac{\sigma_{01}}{\sigma_{0\lambda}}\right) \quad (2)$$

where A_{01} = 50 s^{-1}, I is the integrated emission area of each transition and σ is the centroid of each transition in the emission spectra.

$$\eta = \frac{A_{rad}}{A_{tot}} \quad (3)$$

where $A_{tot} = k_R + k_{NR} = 1/\tau_{exp}$ (k_R is the radiative decay rate; k_{NR} is the non-radiative decay rate; τ_{exp} is the $^5D_0$ decay time).

Table 1. Elemental analysis data of $Q^+[Ln(\beta\text{-dik})_4]^-$ complexes, where Ln = Eu^{III} or Gd^{III}, Q^+ = $(N(C_2H_5)_4)$, $(N(C_4H_9)_4)$ or $(N(C_{12}H_{25})_2(CH_3)_2)$ and β-dik = tta or bmdm

Compound	Ln found (calcd.) / %	C found (calcd.) / %	H found (calcd.) / %	N found (calcd.) / %
$(N(C_2H_5)_4)^+[Eu(tta)_4]^-$	13.00 (13.02)	41.05 (41.17)	3.09 (3.11)	1.10 (1.20)
$(N(C_2H_5)_4)^+[Gd(tta)_4]^-$	13.21 (13.31)	40.50 (41.00)	3.09 (3.10)	1.10 (1.20)
$(N(C_4H_9)_4)^+[Eu(tta)_4]^-$	11.78 (11.90)	45.05 (45.07)	4.09 (4.10)	1.09 (1.10)
$(N(C_4H_9)_4)^+[Gd(tta)_4]^-$	12.14 (12.24)	44.87 (44.90)	4.09 (4.10)	1.07 (1.09)
$(N(C_{12}H_{25})_2(CH_3)_2)^+[Eu(tta)_4]^-$	10.67 (10.71)	49.04 (49.08)	5.09 (5.11)	0.97 (0.99)
$(N(C_{12}H_{25})_2(CH_3)_2)^+[Gd(tta)_4]^-$	11.00 (11.03)	48.70 (48.90)	5.07 (5.09)	0.97 (0.98)
$(N(C_2H_5)_4)^+[Eu(bmdm)_4]^-$	9.85 (9.99)	69.53 (69.55)	6.83 (6.90)	0.91 (0.92)
$(N(C_2H_5)_4)^+[Gd(bmdm)_4]^-$	10.27 (10.31)	69.29 (69.31)	6.84 (6.87)	0.90 (0.92)
$(N(C_4H_9)_4)^+[Eu(bmdm)_4]^-$	9.31 (9.31)	69.30 (70.65)	7.34 (7.41)	0.81 (0.86)
$(N(C_4H_9)_4)^+[Gd(bmdm)_4]^-$	9.57 (9.60)	70.40 (70.43)	7.28 (7.39)	0.85 (0.85)
$(N(C_{12}H_{25})_2(CH_3)_2)^+[Eu(bmdm)_4]^-$	8.53 (8.57)	71.72 (71.84)	7.87 (7.96)	0.80 (0.80)
$(N(C_{12}H_{25})_2(CH_3)_2)^+[Gd(bmdm)_4]^-$	8.85 (8.85)	70.62 (71.63)	7.89 (7.94)	0.79 (0.80)

tta: 2-thenoyltrifluoracetone; bmdm: 1-(4-*tert*-butylphenyl)-3-(4-methoxyphenyl)propane-1,3-dione.

Ground state geometries and theoretical calculations

Sparkle/RM1[44] and Sparkle/PM6[45] models were used to determine the complexes ground state geometries. In this model the lanthanide ion is replaced by a +3e point charge.[46] The restricted Hartree-Fock (RHF) wave functions were optimized using the Broyden-Fletcher-Goldfarb-Shanno (BFGS) procedure with a convergence criterion of 0.15 kcal mol^{-1} $Å^{-1}$ and the semi empirical RM1 (or PM6) with convergence criteria of 10^{-6} kcal mol^{-1} for the self consistent field (SCF). In Mopac2012 package[47] the following keywords were used: RM1 (or PM6), SPARKLE, XYZ, SCFCRT=1D-10, GEO-OK, BFGS, CHARGE=-1, PRECISE, GNORM=0.15 and T=1D. The theoretical JO intensity parameters were calculated using the adequate equations and adjusting, in the physical acceptable range,[43] the polarizability (α) and the charge factors (g) of the ligands in order to fit the theoretical JO intensity parameters with the experimental ones. The excited states calculations were performed in the ORCA software[48] using the INDO/S-CIS with the lanthanide replaced by a +3e point charge.[43,46,49] The transfer and back transfer energy rates from ligands triplet levels to $^5D_{1,0}$ Eu^{III} levels as well as the theoretical quantum efficiency and quantum yield were calculated using the adequate kinetics equations described by Malta *et al.*[50-52] implemented in the LUMPAC software.[53]

Results and Discussion

The stoichiometry of the complexes was confirmed by elemental analysis and lanthanide complexometric titration (Experimental section, Table 1). The thermogravimetric (TG) behaviors of the complexes synthesized in this work are similar. For this reason, only the curves of the $(N(C_2H_5)_4)^+[Eu(tta)_4]^-$ and $(N(C_2H_5)_4)^+[Eu(bmdm)_4]^-$ are shown in Figure 1. The plateau observed between 90-170 °C confirms the absence of coordinated water molecules. The decomposition of the complexes takes place between 300-470 °C, which indicates good thermal stability. Further heating to temperatures higher than 500 °C results in a plateau due to the formation of Eu_2O_3. The residual mass calculated is in agreement with the experimental ones (Table 2), which confirms the proposed stoichiometry.

In the IR spectra, Eu^{III} complexes exhibited noticeable changes in comparison with those of the β-diketone ligands (tta or bmdm). Their characteristic absorption peaks were summarized in Table S1 (Supplementary Information (SI) section). In complexes, the strong C=O stretching vibrations in the regions of 1600-1597 cm^{-1} were red shifted 27-16 cm^{-1} with respect to those of the β-diketones, and new absorption peaks were observed at the region of 1480-1504 cm^{-1}, which ascribed to the enolic C=C stretching vibrations of tetrakis complexes. The FTIR spectra of Gd^{III} complexes showed similar profiles to the Eu^{III} ones (Figure 2).

The phosphorescence spectra of Gd^{III} complexes give information about the triplet level position of the enolate ligands. As the phosphorescence is, in general, quenched at room temperature, for these coordination compounds, it is necessary to record at low temperature (77 K). Gd^{III} complexes are used due to the intrinsic spectroscopic characteristics of the Gd^{III} ion, since there is a large energy

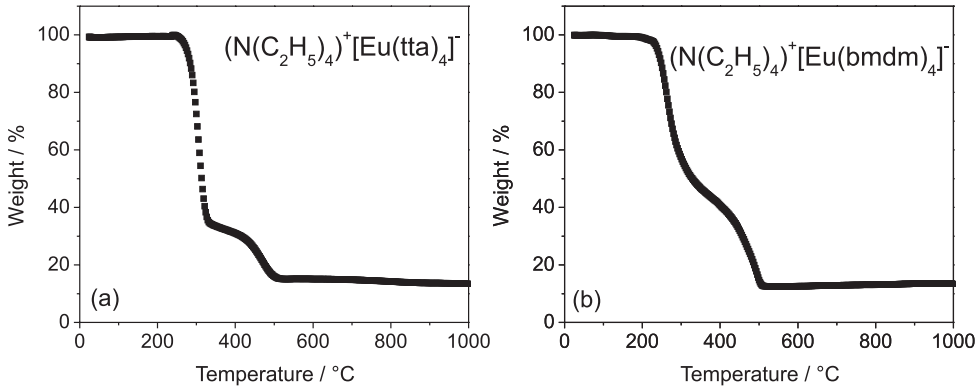

Figure 1. TG curves of (a) $(N(C_2H_5)_4)^+[Eu(tta)_4]^-$ and (b) $(N(C_2H_5)_4)^+[Eu(bmdm)_4]^-$ complexes.

Table 2. Calculated and experimental residual mass obtained for $(N(C_2H_5)_4)^+[Eu(tta)_4]^-$ and $(N(C_2H_5)_4)^+[Eu(bmdm)_4]^-$ complexes

Complex	Molar mass / (g mol^{-1})	Residual mass calculated / %	Residual mass experimental / %
$(N(C_2H_5)_4)^+[Eu(tta)_4]^-$	1202.96	14.63	14.18
$(N(C_2H_5)_4)^+[Eu(bmdm)_4]^-$	1551.77	11.34	12.09

tta: 2-thenoyltrifluoracetone; bmdm: 1-(4-*tert*-butylphenyl)-3-(4-methoxyphenyl)propane-1,3-dione.

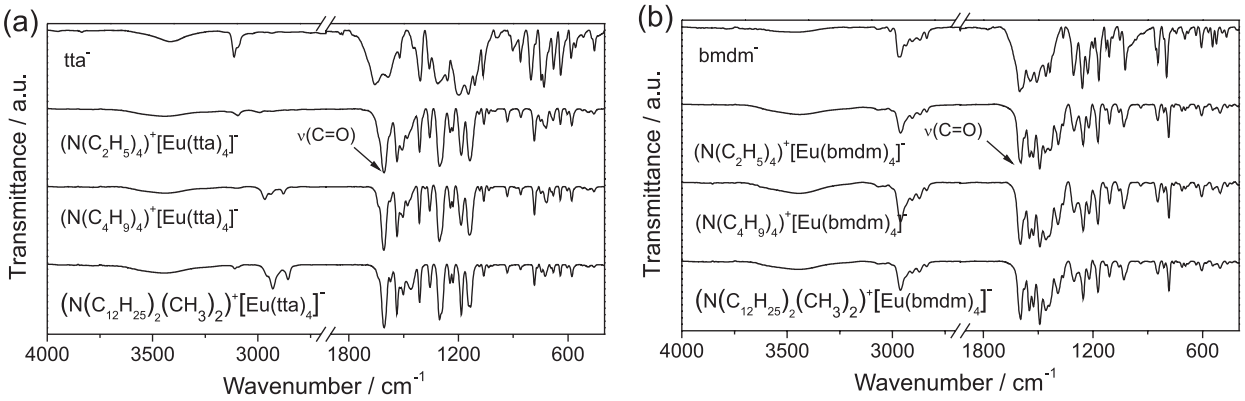

Figure 2. FTIR spectra of the $Q^+[Eu(\beta\text{-dik})_4]^-$ complexes and the ligands. (a) β-dik = tta; (b) β-dik = bmdm.

gap (ca. 32000 cm^{-1}) between $^8S_{7/2}$ ground state and the first $^6P_{7/2}$ excited state of the Gd^{III} ion, it cannot be widened by energy from the lower-laying first excited T_1 state of the β-diketonate ligands via intramolecular ligand-to-metal energy transfer.

The energy of the triplet level of the ligands was determined using the analogous Gd^{III} complex and was found to be located at 19100 cm^{-1}. This value is similar to the one reported in the literature[38] for the tta and bmdm ligands. This result confirms that both ligands (tta and bmdm) are suitable antennas for Eu^{III}.

The excitation spectra of the $Q^+[(Eu(\beta\text{-dik})_4]^-$ complexes had been acquired in the wavelength range 250 to 500 nm, monitoring the characteristic emission $^5D_0 \rightarrow {}^7F_2$ of the Eu^{III} ion at 612 nm. It is clear from the spectra that all the tetrakis complexes have a broad band absorption in the range of 250-400 nm, which is ascribed to the absorption to the β-diketone ligands overlapped with those narrow bands from the Eu^{III} ion attributed to the $^7F_0 \rightarrow {}^5D_4$, $^7F_0 \rightarrow {}^5L_7$, and $^7F_0 \rightarrow {}^5D_3$ transitions. The excitation spectra of the tetrakis complexes also present narrow bands, corresponding to intra-configurational 4f-4f transitions ($^5D_2 \leftarrow {}^7F_0$ ca. 464 nm). This result indicates that the luminescence of the Eu^{III} β-diketonate complexes is a consequence of the sensitization of the europium excited state (Figures 3a and 3b).

The emission spectra of the $Q^+[(Eu(tta)_4]^-$ and $Q^+[(Eu(bmdm)_4]^-$ complexes are shown in Figures 4a and 4b, respectively. In all cases all the $^5D_0 \rightarrow {}^7F_J$ (J = 0-4) transitions are observed, being the $^5D_0 \rightarrow {}^7F_2$ the most intense. The higher intensity of the $^5D_0 \rightarrow {}^7F_2$ transition compared with the $^5D_0 \rightarrow {}^7F_1$ ones means the absence of an inversion center around the Eu^{III} in the complexes, which means that the forced electric dipole and dynamic coupling mechanisms are stronger than the magnetic dipole ones.[6] The number of splittings for each $^5D_0 \rightarrow {}^7F_J$ transition is correlated with the symmetry around the Eu^{III}.[54] The emission spectra of the $Q^+[(Eu(tta)_4]^-$ and $Q^+[(Eu(bmdm)_4]^-$ complexes showed a low number of splittings for each $^5D_0 \rightarrow {}^7F_J$ transition, which means high symmetry around the Eu^{III}. The increase of the carbon chain in the counterion decreases the symmetry around the Eu^{III} in the series $Q^+[(Eu(tta)_4]^-$. This fact was evidenced by the appearance of a second component in the $^5D_0 \rightarrow {}^7F_2$

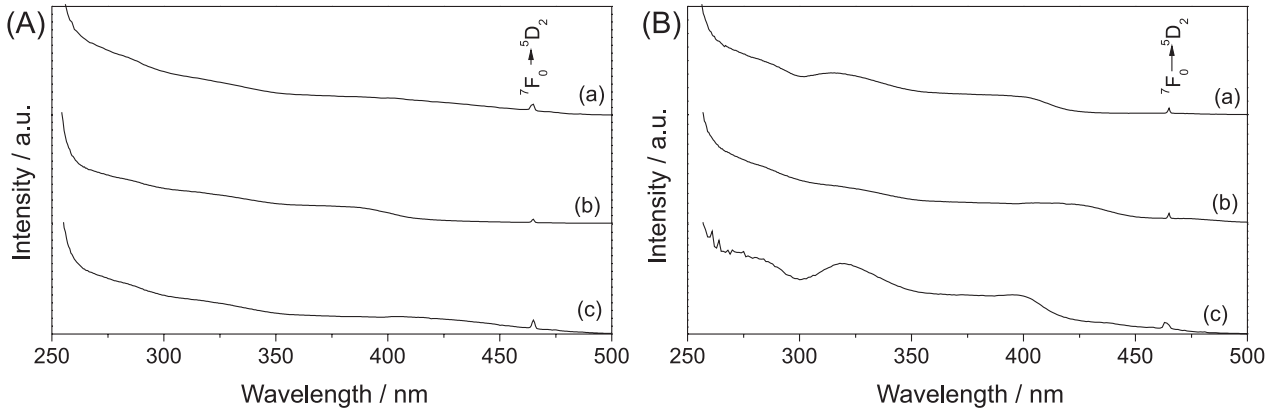

Figure 3. Excitation spectra of the $Q^+[Eu(\beta\text{-dik})_4]^-$ complexes and the ligands. (A) β-dik = tta; (B) β-dik = bmdm. In all cases: (a) $(N(C_2H_5)_4)^+$; (b) $(N(C_4H_9)_4)^+$; (c) $(N(C_{12}H_{25})_2(CH_3)_2)^+$.

(at ca. 619 nm, Figure 4a). That suggests the counterion, even outside the first coordination sphere, can disturb the symmetry around the Eu^{III} in this series. The effect of the counterion was also observed in the series of complexes $Q^+[(Eu(bmdm)_4]^-$. However, the changes are smaller than the tta series. To gain more insight about the changes in the point symmetry, the JO intensity parameters[55,56] were obtained and are shown in Table 3.

The JO intensity parameters Ω_2 and Ω_4 are strongly correlated with the symmetry around the Ln^{III} ion.[57-59] In the $Q^+[Eu(tta)_4]^-$ series the value of the Ω_2 intensity parameter increased, while the Ω_4 ones decreased, which means that there was a decrease in the microsymmetry along the series. This result corroborates with the previous discussion about the emission spectra. The interactions ion-dipole between the $-CF_3$ groups from the tta ligand with the counterion might explain the distortions in the symmetry around the Eu^{III} in the series $Q^+[Eu(tta)_4]^-$. In the $Q^+[Eu(bmdm)_4]^-$ series the trend in the JO intensity parameters values was the opposite and the changes smaller compared with the $Q^+[Eu(tta)_4]^-$ series. Probably the bulky lateral groups of the bmdm ligand (*tert*-butyl and methoxy) insulate the Eu^{III} from the influence of the counterion and have weak interactions with the alkyl chains of the counterion. Carlos and co-workers[60] also observed the counterion effect in the symmetry around the Eu^{III} in the complexes $Q^+[Eu(NTA)_4]^-$ (Q = tetrabutylammonium, 1-butyl-3-methylimidazolium, and 1-butyl-3-methylpyridinium and NTA = naphtoyltrifluoroacetonato).

The emission lifetime values (τ) of Eu^{III} compounds have a direct correlation with the non-radiative processes promoted by high energy oscillators close to the metal, such as C–H, N–H and/or O–H.[61] The emission lifetime value trend across the $Q^+[Eu(tta)_4]^-$ and $Q^+[Eu(bmdm)_4]^-$ series were the same. The highest τ was found for the complexes containing the $(N(C_4H_9)_4)^+$ cation, while the lowest one was found for the complexes containing the $(N(C_{12}H_{25})_2(CH_3)_2)^+$ cation. The lowest emission lifetime found for the complexes containing the $(N(C_{12}H_{25})_2(CH_3)_2)^+$ cation is due to the high number of C–H oscillators. The lower emission lifetime values of the $Q^+[Eu(bmdm)_4]^-$ series compared with the $Q^+[Eu(tta)_4]^-$ ones are explained by the presence of more C–H oscillators in the structure of the bmdm ligand. In this particular case the distance Eu–Eu may also be a factor in the deactivation; however, we were not able to quantify this effect.

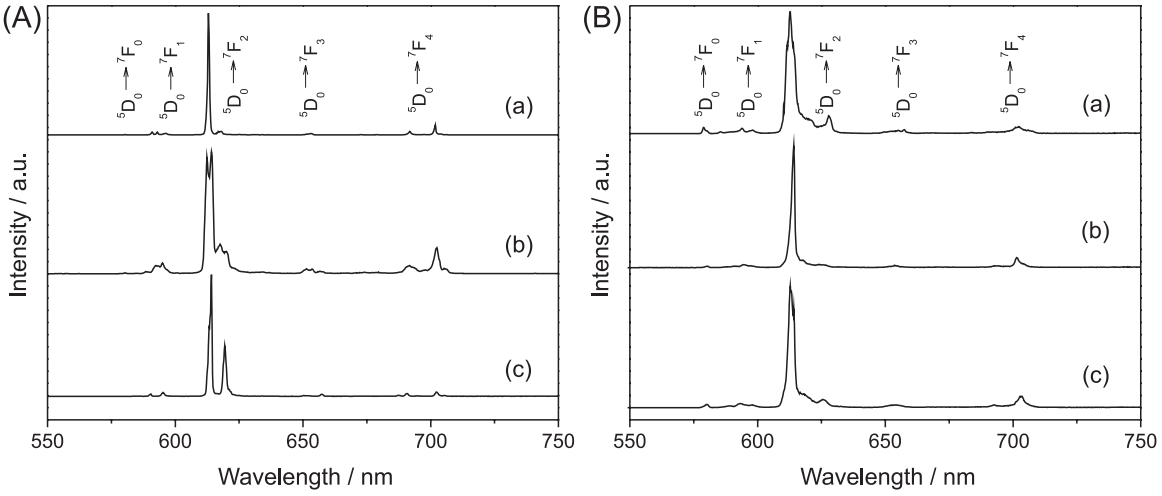

Figure 4. Emission spectra of the $Q^+[Eu(\beta\text{-dik})_4]^-$ complexes and the ligands. (A) β-dik = tta; (B) β-dik = bmdm. In all cases: (a) $(N(C_2H_5)_4)^+$; (b) $(N(C_4H_9)_4)^+$; (c) $(N(C_{12}H_{25})_2(CH_3)_2)^+$.

Table 3. Judd-Ofelt (JO) intensity parameters (Ω_2 and Ω_4), radiative rates (A_{rad}), emission lifetime of the Eu^{III} complexes (τ) and quantum efficiency (η)

Complex	$\Omega_2 \times 10^{-20}$ / cm^2	$\Omega_4 \times 10^{-20}$ / cm^2	A_{rad} / s^{-1}	τ / ms	η / %
$(N(C_2H_5)_4)^+[Eu(tta)_4]^-$	22.5	7.0	816	0.81	66
$(N(C_4H_9)_4)^+[Eu(tta)_4]^-$	23.2	6.7	865	1.04	90
$(N(C_{12}H_{25})_2(CH_3)_2)^+[Eu(tta)_4]^-$	38.8	5.4	1306	0.41	54
$(N(C_2H_5)_4)^+[Eu(bmdm)_4]^-$	28.1	5.4	993	0.57	56
$(N(C_4H_9)_4)^+[Eu(bmdm)_4]^-$	24.2	5.8	860	0.68	59
$(N(C_{12}H_{25})_2(CH_3)_2)^+[Eu(bmdm)_4]^-$	23.0	6.4	835	0.29	24

tta: 2-thenoyltrifluoracetone; bmdm: 1-(4-*tert*-butylphenyl)-3-(4-methoxyphenyl)propane-1,3-dione.

The ground state geometry of the complexes was determined using the Sparkle/RM1[44] and Sparkle/PM6[45] methods implemented in the Mopac2012 software[47] (Figures 5 and 6, and Figures S3 and S4, SI section). The average Eu–O distance bond obtained by X-ray diffraction for $[Eu(\beta\text{-dik})_4]^-$ complexes is 2.3878 Å,[55,57-62] while using the Sparkle/RM1 and Sparkle/PM6 we obtained 2.4589 (2.98% error) and 2.4306 Å (1.79% error), respectively.[60,62-67] Therefore, the Sparkle/PM6 method gave better values for the Eu–O distance bond than the Sparkle/RM1 in this case.

The theoretical JO intensity parameters (Table 4) are in good agreement with the ones obtained experimentally (Table 3). The calculated energy transfer from the triplet level of the ligand (T) to the $^5D_{1,0}$ levels of the Eu^{III} were obtained using the equations developed by Malta and co-workers[50-52] and are summarized in Table 5. The energy transfer rates $T \rightarrow {}^5D_{1,0}$ are one order of magnitude higher for the $Q^+[Eu(tta)_4]^-$ series compared with the $Q^+[Eu(bmdm)_4]^-$ ones. The energy transfer rates are influenced by the energy of the triplet level of the ligand and the distance donor-acceptor (R_L).[10] In the present case, the energy of the triplet level of both ligands is similar (ca. 19100 cm^{-1}), but the calculated R_L value for the $Q^+[Eu(tta)_4]^-$ series is lower than the $Q^+[Eu(bmdm)_4]^-$ ones (Table 5). That explains the highest energy transfer values obtained for the $Q^+[Eu(tta)_4]^-$ series. The theoretical quantum yield (Φ_{calc}) depends on the combination of energy transfer and back transfers rates and the quantum efficiency (η). In the present case the highest value for the $Q^+[Eu(tta)_4]^-$ series, compared with the $Q^+[Eu(bmdm)_4]^-$ ones, is a combination of the higher energy transfer (due to the smaller R_L) and quantum efficiency (due to the absence of high-energy oscillators) (Table 5).

Conclusions

A series of $Q^+[Ln(\beta\text{-dik})_4]^-$ complexes that are thermally stable (Figure 1) and display strong red luminescence upon excitation centered in the ligands bands (Figures 3 and 4) were synthesized. We provided evidence based on the emission spectra and the calculation of the experimental JO intensity parameters (Table 4) that the point symmetry around the Eu^{III} can be disturbed by the interaction between the lateral groups of the ligands (tta or bmdm) and the counterion. The complexes have distorted

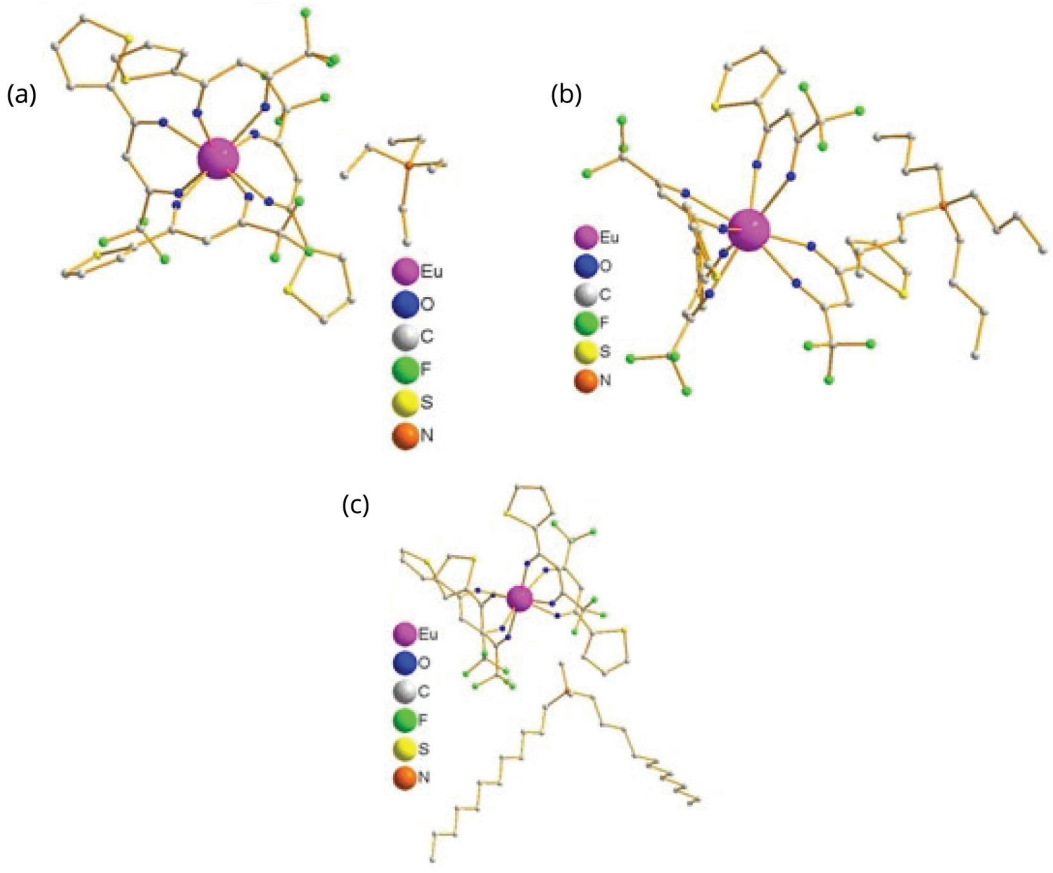

Figure 5. Ground state geometry of the (a) $(N(C_2H_5)_4)^+[Eu(tta)_4]^-$; (b) $(N(C_4H_9)_4)^+[Eu(tta)_4]^-$ and (c) $(N(C_{12}H_{25})_2(CH_3)_2)^+[Eu(tta)_4]^-$ complexes obtained by the Sparkle/RM1.

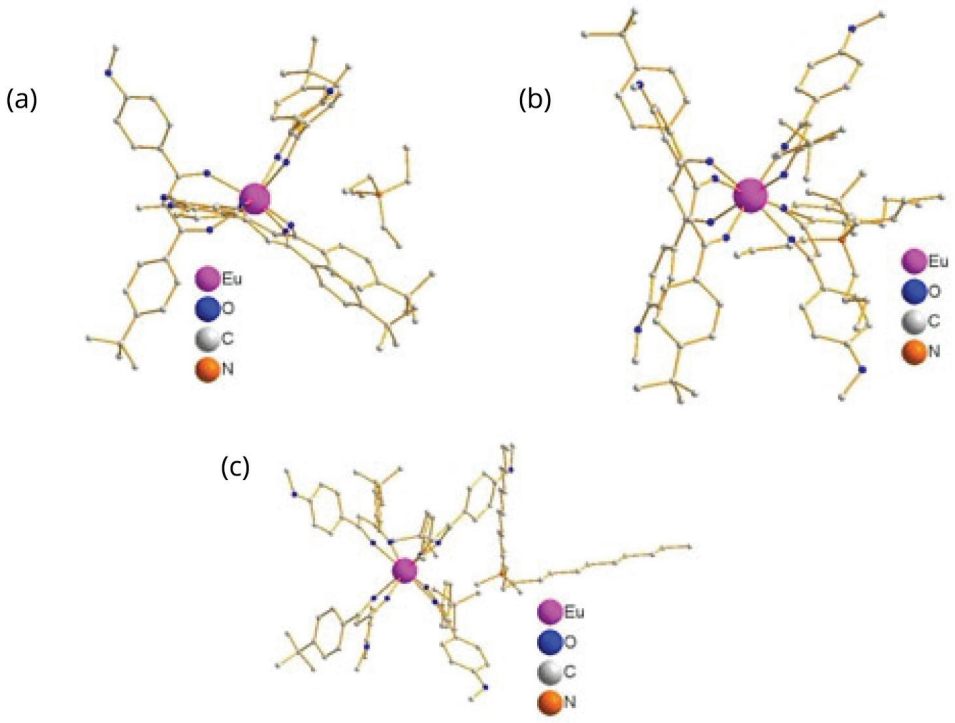

Figure 6. Ground state geometry of the (a) $(N(C_2H_5)_4)^+[Eu(bmdm)_4]^-$; (b) $(N(C_4H_9)_4)^+[Eu(bmdm)_4]^-$ and (c) $(N(C_{12}H_{25})_2(CH_3)_2)^+[Eu(bmdm)_4]^-$ complexes obtained by the Sparkle/RM1.

Table 4. Theoretical Judd-Ofelt (JO) intensity parameters

Complex	$(\Omega_2)_{theo} \times 10^{-20}$ / cm^2	$(\Omega_2)_{exp} \times 10^{-20}$ / cm^2	$(\Omega_4)_{theo} \times 10^{-20}$ / cm^2	$(\Omega_4)_{exp} \times 10^{-20}$ / cm^2	$(\Omega_6)_{theo} \times 10^{-20}$ / cm^2
$(N(C_2H_5)_4)^+[Eu(tta)_4]^-$	23	22	5.0	7.0	0.20
$(N(C_4H_9)_4)^+[Eu(tta)_4]^-$	23	23	6.7	6.7	0.14
$(N(C_{12}H_{25})_2(CH_3)_2)^+[Eu(tta)_4]^-$	39	39	5.8	5.4	0.69
$(N(C_2H_5)_4)^+[Eu(bmdm)_4]^-$	28	28	5.4	5.4	0.22
$(N(C_4H_9)_4)^+[Eu(bmdm)_4]^-$	24	24	5.8	5.8	0.13
$(N(C_{12}H_{25})_2(CH_3)_2)^+[Eu(bmdm)_4]^-$	22	23	8.0	6.4	1.33

$(\Omega_2)_{theo}$, $(\Omega_4)_{theo}$, $(\Omega_6)_{theo}$: Judd-Ofelt theoretical intensity parameters; $(\Omega_2)_{exp}$, $(\Omega_4)_{exp}$: Judd-Ofelt experimental intensity parameters; tta: 2-thenoyltrifluoracetone; bmdm: 1-(4-*tert*-butylphenyl)-3-(4-methoxyphenyl)propane-1,3-dione.

Table 5. Transfer and back transfer rates

Complex	$T \rightarrow {}^5D_1$ / s^{-1}	$T \leftarrow {}^5D_1$ / s^{-1}	$T \rightarrow {}^5D_0$ / s^{-1}	$T \leftarrow {}^5D_{10}$ / s^{-1}	R_L / Å	Φ_{theo} / %
$(N(C_2H_5)_4)^+[Eu(tta)_4]^-$	5.1×10^4	8.3×10^2	6.6×10^4	2.6×10^{-1}	4.6283	34.6
$(N(C_4H_9)_4)^+[Eu(tta)_4]^-$	5.0×10^4	5.4×10^2	6.3×10^4	1.7×10^{-1}	4.6313	45.9
$(N(C_{12}H_{25})_2(CH_3)_2)^+[Eu(tta)_4]^-$	3.4×10^4	7.7×10^1	4.0×10^4	2.2×10^{-2}	4.7202	22.6
$(N(C_2H_5)_4)^+[Eu(bmdm)_4]^-$	4.0×10^3	3.3×10^{-1}	4.0×10^3	8.3×10^{-5}	5.2547	4.1
$(N(C_4H_9)_4)^+[Eu(bmdm)_4]^-$	3.8×10^3	5.5×10^{-1}	3.9×10^3	1.4×10^{-4}	5.2831	4.1
$(N(C_{12}H_{25})_2(CH_3)_2)^+[Eu(bmdm)_4]^-$	3.3×10^3	6.4×10^{-1}	3.5×10^3	1.6×10^{-4}	5.3218	1.6

T: triplet level of the ligand; R_L: distance of donor-acceptor; Φ_{theo}: theoretical quantum yield; tta: 2-thenoyltrifluoracetone; bmdm: 1-(4-*tert*-butylphenyl)-3-(4-methoxyphenyl)propane-1,3-dione.

square antiprismatic geometry as predicted by semi-empirical Sparkle/RM1 and Sparkle/PM6 models. The theoretically calculated results are in excellent agreement with the experimental results, which demonstrates the effectiveness of the semi-empirical calculation in predicting the photophysical properties. The lifetime of the excited state $^5D_0$ and quantum efficiency of the Eu^{III} complexes are influenced by the different lengths of ammonium alkyl chains. The lower emission lifetime values of the $Q^+[Eu(bmdm)_4]^-$ series (0.29-0.68 ms) is explained by the

presence of more C–H oscillators in its structure quantum efficiency (η = 24-59%). Our results indicate that JO parameters provided us some insights on the behavior of specific groups in their optical properties, *tert*-butyl and methoxy groups from bmdm ligand insulate Eu^{III} from the influence of Q = $(N(C_4H_9)_4)^+$, τ = 1.04 ms and η = 90%. Furthermore, the lowest values of the distance donor-acceptor (R_L) were obtained for the $Q^+[Eu(tta)_4]^-$ series, which reflected in a higher energy transfer rate ligand → Eu^{III} when compared with the $Q^+[Eu(bmdm)_4]^-$ ones (Table 5), which is an important contribution of this study.

This work is a result of the chemical design directed by theoretical calculations, used as a tool to predict and interpret photoluminescent properties. The study of the counterion-tetrakis Ln^{III} complexes with distint β-diketones (tta or bmdm) and correlations with intermolecular forces allows the control over the packing density of molecules. Here we evaluated by spectroscopic data and theoretical methods that will guide further development of new stable LB films applied as emissive layers in displays.

Supplementary Information

Supplementary information is available free of charge at http://jbcs.sbq.org.br as PDF file.

Acknowledgments

The authors thank CAPES, CNPq and FAPESP (Brazilian agencies) for the financial support. R. D. A. thanks CAPES for the scholarship.

References

1. Bünzli, J.-C. G. In *Luminescence of Lanthanide Ions in Coordination Compounds and Nanomaterials*; de Bettencourt-Dias, A., ed.; Wiley: New Jersey, USA, 2014, p. 125.
2. Bünzli, J.-C. G.; *Chem. Rev.* **2010**, *110*, 2729.
3. Eliseeva, S. V.; Bünzli, J.-C. G.; *Chem. Soc. Rev.* **2010**, *39*, 189.
4. Binemanns, K. In *Handbook on the Physics and Chemistry of Rare Earths*; Gschneidner Jr., K. A.; Bünzli, J.-C. G.; Pecharsky, V. K., eds.; North-Holland: Elsevier, 2005, p. 111-272.
5. de Bettencourt-Dias, A. In *Luminescence of Lanthanide Ions in Coordination Compounds and Nanomaterials*; de Bettencourt-Dias, A., ed.; Wiley: New Jersey, USA, 2014, p. 1.
6. Bünzli, J.-C. G.; Eliseeva, S. V. In *Lanthanide Luminescence: Photophysical, Analytical and Biological Aspects*; Hänninen, P.; Härmä, H., eds.; Springer: Berlin, Germany, 2011, p. 1.
7. Chauvin, A.-S.; Comby, S.; Song, B.; Vandevyver, C. D. B.; Bünzli, J.-C. G.; *Chem. Eur. J.* **2008**, *14*, 1726.
8. Deiters, E.; Song, B.; Chauvin, A.-S.; Vandevyver, C. D. B.; Gumy, F.; Bunzli, J.-C. G.; *Chem. Eur. J.* **2009**, *15*, 885.
9. D'Aleo, A.; Picot, A.; Baldeck, P. L.; Andraud, C.; Maury, O.; *Inorg. Chem.* **2008**, *47*, 10269.
10. Monteiro, J. H. S. K.; de Bettencourt-Dias, A.; Sigoli, F. A.; *Inorg. Chem.* **2016**, *55*, 9954.
11. de Bettencourt-Dias, A.; Barber, P. S.; Bauer, S.; *J. Am. Chem. Soc.* **2012**, *134*, 6987.
12. de Bettencourt-Dias, A.; Barber, P. S.; Viswanathan, S.; de Lill, D. T.; Rollett, A.; Ling, G.; Altun, S.; *Inorg. Chem.* **2010**, *49*, 8848.
13. Bauer, H.; Blanc, J.; Ross, D. L.; *J. Am. Chem. Soc.* **1964**, *86*, 5125.
14. Guedes, M. A.; Paolini, T. B.; Felinto, M. C. F. C.; Kai, J.; Nunes, L. A. O.; Malta, O. L.; Brito, H. F.; *J. Lumin.* **2011**, *131*, 99.
15. Xiong, R. G.; You, X. Z.; *Inorg. Chem. Commun.* **2002**, *5*, 677.
16. Lunstroot, K.; Driesen, K.; Nockemann, P.; Gorller-Walrand, C.; Binnemans, K.; Bellayer, S.; Le Bideau, J.; Vioux, A.; *Chem. Mater.* **2006**, *18*, 5711.
17. Hehlen, M. P.; Brik, M. G.; Kramer, K. W.; *J. Lumin.* **2013**, *136*, 221.
18. Yan, B.; Xu, B.; *J. Fluoresc.* **2005**, *15*, 619.
19. Raji, R.; Kumar, R. G. A.; Gopchandran, K. G.; *J. Lumin.* **2019**, *205*, 179.
20. Wang, D.; Liu, H.; Fan, L.; Yin, G.; Zheng, J.; *Synth. Met.* **2015**, *209*, 267.
21. Ciric, A.; Stojadinovic, S.; Sekulic, M.; Dramicanin, M. D.; *J. Lumin.* **2019**, *205*, 351.
22. Quirino, W. G.; Adati, R. D.; Lima, S. A. M.; Legnani, C.; Jafelicci, M.; Davolos, M. R.; Cremona, M.; *Thin Solid Films* **2006**, *515*, 927.
23. Biju, S.; Xu, L. J.; Sun, C. Z.; Chen, Z. N.; *J. Mater. Chem. C* **2015**, *3*, 5775.
24. Martins, J. P.; Martin-Ramos, P.; Coya, C.; Alvarez, A. L.; Pereira, L. C.; Diaz, R.; Martin-Gil, J.; Silva, M. R.; *Mater. Chem. Phys.* **2014**, *147*, 1157.
25. Zhang, L.; Li, B.; *J. Lumin.* **2009**, *129*, 1304.
26. Reyes, R.; Hering, E. N.; Cremona, M.; da Silva, C. F. B.; Brito, H. F.; Achete, C. A.; *Thin Solid Films* **2002**, *420*, 23.
27. Ariga, K.; Yamauchi, Y.; Mori, T.; Hill, J. P.; *Adv. Mater.* **2013**, *25*, 6477.
28. Clemente-Leon, M.; Coronado, E.; Soriano-Portillo, A.; Mingotaud, C.; Dominguez-Vera, J. M.; *Adv. Colloid Interface Sci.* **2005**, *116*, 193.
29. Wang, J.; Wang, H. S.; Liu, F. Y.; Fu, L. S.; Zhang, H. J.; *J. Lumin.* **2003**, *101*, 63.
30. Ito, T.; Yamase, T.; *J. Alloys Compd.* **2006**, *408*, 813.
31. Petty, M. C.; *Langmuir-Blodgett Films: An Introduction*; Cambridge University Press: New York, USA, 1996.
32. Petty, M. C.; *Molecular Electronics: From Principles to Practice*; Wiley: Chichester, England, 2007.

33. Jung, G. Y.; Yates, A.; Samuel, I. D. W.; Petty, M. C.; *Mater. Sci. Eng., C* **2001**, *14*, 1.
34. Gambinossi, F.; Baglioni, P.; Caminati, G.; *Mater. Sci. Eng., C* **2007**, *27*, 1056.
35. Casu, M. B.; Imperia, P.; Schrader, S.; Schulz, B.; Fangmeyer, F.; Schürmann, H.; *Stud. Interface Sci.* **2001**, *11*, 121.
36. Pavier, M. A.; Weaver, M. S.; Lidzey, D.; Richardson, T.; Searle, T. M.; Bradley, D. D. C.; Huang, C. H.; Li, H.; Zhou, D.; *Thin Solid Films* **1996**, *284*, 644.
37. Era, M.; Tsutsui, T.; Takehara, K.; Isomura, K.; Taniguchi, H.; *Thin Solid Films* **2000**, *363*, 229.
38. Adati, R. D.; Pavinatto, F. J.; Monteiro, J. H. S. K.; Davolos, M. R.; Jafelicci, M.; Oliveira, O. N.; *New J. Chem.* **2012**, *36*, 1978.
39. Zhou, D. J.; Wang, K. Z.; Huang, C. H.; Xu, G. X.; Xu, L. G.; Li, T. K.; *Solid State Commun.* **1995**, *93*, 167.
40. Wang, K. Z.; Gao, L. H.; Huang, C. H.; Yao, G. Q.; Zhao, X. S.; Xia, X. H.; Xu, J. M.; Li, T. K.; *Solid State Commun.* **1996**, *98*, 1075.
41. Zhou, D. J.; Huang, C. H.; Yao, G. Q.; Bai, J.; Li, T. K.; *J. Alloys Compd.* **1996**, *235*, 156.
42. Melby, L. R.; Abramson, E.; Caris, J. C.; Rose, N. J.; *J. Am. Chem. Soc.* **1964**, *86*, 5117.
43. de Sá, G. F.; Malta, O. L.; Donegá, C. M.; Simas, A. M.; Longo, R. L.; Santa-Cruz, P. A.; da Silva, E. F.; *Coord. Chem. Rev.* **2000**, *196*, 165.
44. Filho, M. A. M.; Dutra, J. D. L.; Rocha, G. B.; Freire, R. O.; Simas, A. M.; *RSC Adv.* **2013**, *3*, 16747.
45. Freire, R. O.; Simas, A. M.; *J. Chem. Theory Comput.* **2010**, *6*, 2019.
46. de Andrade, A. V. M.; da Costa, N. B.; Simas, A. M.; de Sá, G. F.; *Chem. Phys. Lett.* **1994**, *227*, 349.
47. Stewart, J. J. P.; *MOPAC2012*; Springs, Colorado, USA, 2012.
48. Neese, F.; *Wiley Interdiscip. Rev.: Comput. Mol. Sci.* **2012**, *2*, 73.
49. Ridley, J. E.; Zerner, M. C.; *Theor. Chim. Acta* **1976**, *42*, 223.
50. Malta, O. L.; *J. Lumin.* **1997**, *71*, 229.
51. Malta, O. L.; Gonçalves e Silva, F. R.; *Spectrochim. Acta, Part A* **1998**, *54*, 1593.
52. Malta, O. L.; *J. Non-Cryst. Solids* **2008**, *354*, 4770.
53. Dutra, J. D. L.; Bispo, T. D.; Freire, R. O.; *J. Comput. Chem.* **2014**, *35*, 772.
54. Tanner, P. A. In *Lanthanide Luminescence: Photophysical, Analytical and Biological Aspects*; Hänninen, P.; Härmä, H., eds.; Springer: Berlin, Germany, 2011, p. 183.
55. Judd, B. R.; *Phys. Rev.* **1962**, *127*, 750.
56. Ofelt, G. S.; *J. Chem. Phys.* **1962**, *37*, 511.
57. Ferreira, R. A. S.; Nobre, S. S.; Granadeiro, C. M.; Nogueira, H. I. S.; Carlos, L. D.; Malta, O. L.; *J. Lumin.* **2006**, *121*, 561.
58. Monteiro, J. H. S. K.; Formiga, A. L. B.; Sigoli, F. A.; *J. Lumin.* **2014**, *154*, 22.
59. Monteiro, J. H. S. K.; de Bettencourt-Dias, A.; Mazali, I. O.; Sigoli, F. A.; *New J. Chem.* **2015**, *39*, 1883.
60. Bruno, S. M.; Ferreira, R. A.; Paz, F. A. A.; Carlos, L. D.; Pillinger, M.; Ribeiro-Claro, P.; Gonçalves, I. S.; *Inorg. Chem.* **2009**, *48*, 4882.
61. Bünzli, J.-C. G.; *Coord. Chem. Rev.* **2015**, *293*, 19.
62. Yi, S. J.; Yao, M. H.; Wang, J.; Chen, X.; *Phys. Chem. Chem. Phys.* **2016**, *18*, 27603.
63. Burns, J. H.; Danford, M. D.; *Inorg. Chem.* **1969**, *8*, 1780.
64. Goossens, K.; Nockemann, P.; Driesen, K.; Goderis, B.; Gorller-Walrand, C.; Van Hecke, K.; Van Meervelt, L.; Pouzet, E.; Binnemans, K.; Cardinaels, T.; *Chem. Mater.* **2008**, *20*, 157.
65. Zhang, G. C.; Li, D. D.; Kong, M.; Su, J.; Zhou, H. P.; Wu, J. Y.; Tian, Y. P.; *Synth. React. Inorg. Met.-Org. Chem.* **2016**, *46*, 1254.
66. Nockemann, P.; Beurer, E.; Driesen, K.; Van Deun, R.; Van Hecke, K.; Van Meervelt, L.; Binnemans, K.; *Chem. Commun.* **2005**, *34*, 4354.
67. Chen, X. F.; Liu, S. H.; Duan, C. Y.; Xu, Y. H.; You, X. Z.; Ma, J.; Min, N. B.; *Polyhedron* **1998**, *17*, 1883.

Submitted: December 5, 2018
Published online: April 26, 2019